

Sixth Paper

The original paper (in Serbian) appears in monograph "Service Cracks in Pressure Vessels and Storage Tanks," edited by S. Sedmak and A. Sedmak, jointly published by the Faculty of Technology and Metallurgy (Belgrade), European Centre for Peace and Development (Belgrade), and GOŠA Institute (Smederevska Palanka), pp. 211-227, 1994. The monograph contains lectures from the Sixth International Fracture Mechanics Summer School (IFMASS 6) held in Vrdnik, 1991.

Originalna verzija ovog rada objavljena je na srpskom jeziku u monografiji "Eksploatacijske prsline u posudama pod pritiskom i rezervoarima", urednici S. Sedmak i A. Sedmak, zajedničko izdanje Tehnološko-metalurškog fakulteta (Beograd), Evropskog centra za mir i razvoj (Beograd) i Instituta GOŠA (Smederevska Palanka), 1980, str. 211-227. Monografija sadrži predavanja sa Šeste međunarodne letnje škole mehanike loma (IFMASS 6) u Vrdniku, 1991.

Aleksandar Sedmak
Mladen Berković
Nevena Savović

NUMERICAL ANALYSIS OF SURFACE CRACK PROBLEMS IN PRESSURE VESSELS

Original scientific paper UDC: 62-988:539.421:519.6

INTRODUCTION

The purpose of this work is to present the possibilities of the numerical analysis of surface cracks in pressure vessels and also to show the results in certain cases. The paper mainly concerns stationary cracks, while unstable crack growth is considered in other papers of this issue /1,2,3/.

Having in mind the three dimensional character of stress and strain fields around the crack tip and plastic strains of the material used in pressure vessels due to the presence of cracks, it is clear that even stationary cracks represent a complex problem. On the other hand, pressure vessels may generally be observed as a two dimensional (2D) problem (thin shells). This allows certain simplifications of the surface crack problem using quasi-2D or 2D analysis. Hence, further text will be about 3D analysis (application of finite element method – FEM), quasi-2D analysis (integral transformation method and FEM for thin shells combined with a spring model), and 2D analysis (FEM) of surface crack problems. Every method mentioned above includes results obtained by the authors, as well as other results, whose purpose is to fully represent the analysed problem.

THREE DIMENSIONAL ANALYSIS

Linear elastic analysis of surface cracks in flat planes is the starting point in this analysis. The effect of material plasticity and vessel curvature will be shown later. Most work on this problem has been done by Newman and Raju, giving us a number of results obtained by 3D FEM, /4/. Some of these results are given in Figs. 1-3. Figures 1-3 also include the distribution of stress intensity factors (SIF) along the crack front (defined by angle ϕ), as a parameter for different crack depth (defined by non-dimensional quotient c/t , where c is crack depth, and t is plate thickness). Each of these figures is related to a typical crack form (defined by the length–depth ratio, $2a/c$, where $2a$ is the crack length). In Figure 1, $2a/c = 3$, in Fig. 2, $2a/c = 5$, and in Fig. 3, $2a/c = 10$. These figures show that the largest SIF

corresponds to the largest crack depth ($\phi = 90^\circ$) for long (i.e. $2a/c$ is large), and shallow (c/t is small) cracks, which is in accordance with Irvin's analytical expression:

$$K = \frac{1.12\sigma\sqrt{\pi a}}{\sqrt{\phi^2 - 0.212\left(\frac{\sigma}{R_e}\right)^2}} \quad (1)$$

Only in case of short ($2a/c$ is small) and deep cracks (c/t is large), Fig. 1, the largest value of SIF corresponds to angle $\phi = 0^\circ$, i.e. the largest crack length. Therefore, long and shallow cracks will grow along their depth, while relatively short and deep cracks grow along their length. However, the effects of the vessel shape (curvature) and material plasticity on the crack behaviour should also be taken into account.

THE EFFECT OF CURVATURE

Curvature has no significant effect on SIF distribution as we can see from Fig. 1, /5/. This figure shows the distribution of SIF along the front of a longitudinal crack in a cylinder, with radius (R) to thickness (t) ratio of 10. Crack dimensions are chosen to correspond to the case shown in Fig. 3 in order to make comparing of results regarding the effect of curvature easier. It is obvious that there are no differences in the SIF distribution for cases of plates and cylinders, in other words the effect of curvature here is negligible. A more complete analysis of this effect requires results for short cracks and other curve values (R/t), which are not the subject of this paper, except for the case of interfering with the effects of material plasticity.

THE EFFECT OF MATERIAL PLASTICITY

This effect is significant not only as a partially different distribution of the corresponding fracture mechanics parameter (J integral), but also as a so-called local constraint (LC). The local constraint which occurs due to multiaxial stress state can be defined as:

$$LC = \frac{\sigma_m}{\sigma_v} \quad (2)$$

where σ_m is the principle stress, and σ_v is the equivalent (von Mises) stress, /6/.

In /6/, it is shown that the distribution of LC along the crack front has a significant part in the surface crack growth mechanism. Besides, this effect of material plasticity is very important for evaluating the possibilities of applying experimental results obtained from "small" standard specimens to real "large" structures, such as pressured vessels (a more detailed analysis of this problem can be found in /7/). Hence, from this point, we will analyse the effects of LC distribution and J integral along the crack front, in order to evaluate the qualitative and quantitative effects of material plasticity to the surface crack growth in a pressure vessel.

There is only very few data found in literature /1,6-9/ concerning the J integral distribution along the crack front in a plate or a cylinder which are analysed here. All data related to cylindrical vessels were obtained for the case of axial cracks which is of greatest practical interest.

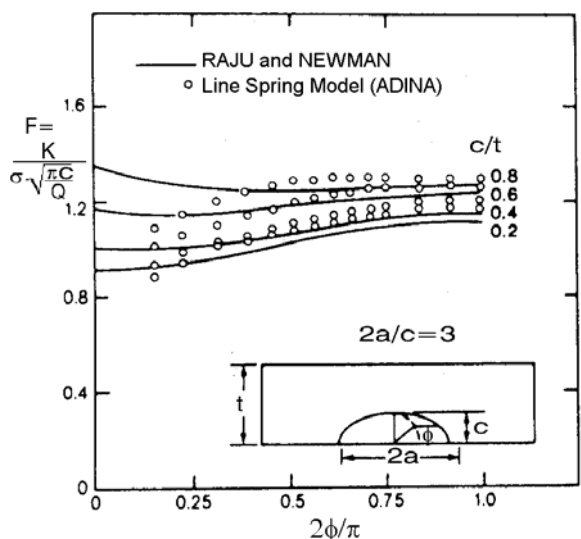


Figure 1. Distribution of SIF along the crack front.

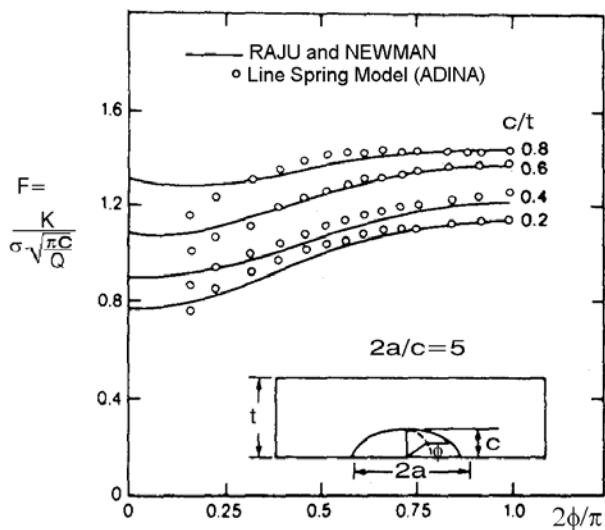


Figure 2. Distribution of SIF along the crack front.

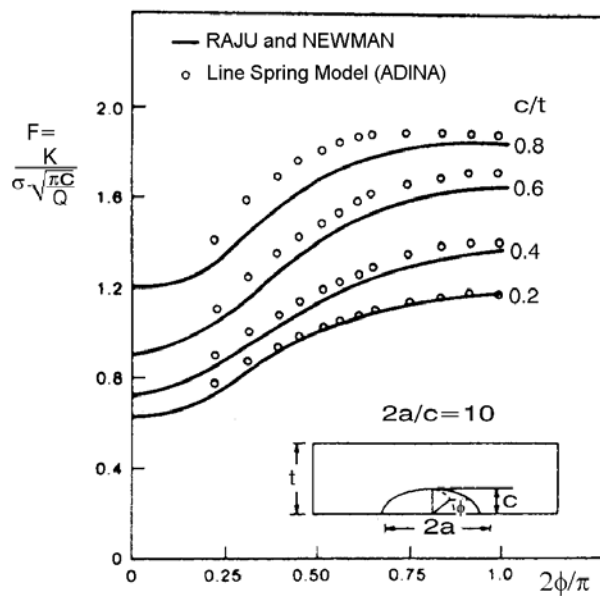


Figure 3. Distribution of SIF along the crack front.

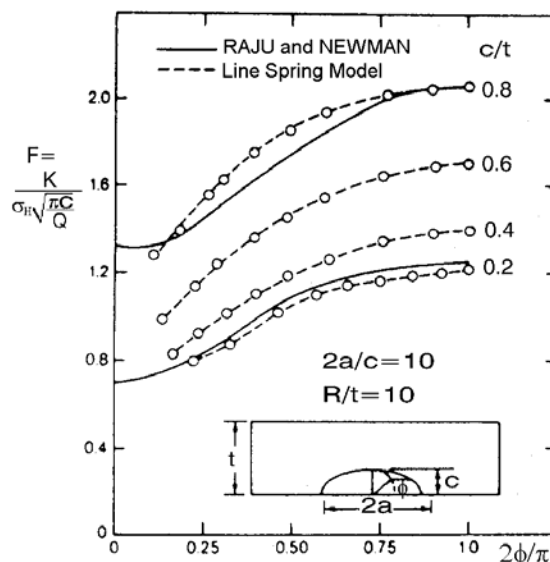


Figure 4. Distribution of SIF along the crack front.

Figure 5 shows results of J integral distribution along the crack front in a cylinder (diameter $D = 3030$ mm, thickness $t = 8$ mm, crack length $2a = 4.28$ mm, crack depth $c = 1.5$ mm) and in a specimen the shape of a tensile plate (of the same thickness) with a central crack (of same dimensions). As we can see from Fig. 5, the distribution of J integral becomes more uneven for remote stress values greater than 600 MPa. Hence, when this stress reaches its greatest value of 1400 MPa, the surface J integral is about 40% less than the J integral at the greatest depth. Additional consideration of these results (Fig. 6) also shows the dual effect of plasticity: J integral value growth and the plane strain state stops to be in effect for conditions on the surface. This results in local growth of yield and a decrease of corresponding J integral values (below the stress that is 75% of yield stress – 1000 MPa) by 7% as well as another growth as loading continues to increase. These results were obtained using the MARC programme, assuming small strains

and material nonlinearity introduced by the Ramberg-Osgood relation $\sigma = K\epsilon^n$. Paper /8/ contains a detailed description and analysis of the results. The same also contains results for LC distribution along the crack front which are given here in Fig. 7 (plate) and in Fig. 8 (cylinder). It is obvious that there are now qualitative differences between these distributions, i.e. the curve effect is in this case negligible.

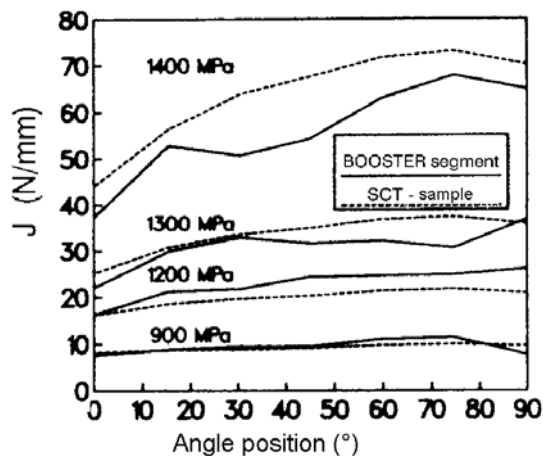


Figure 5. J integral distribution along the crack front.

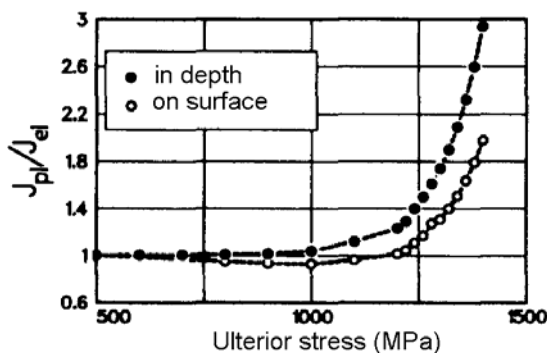


Figure 6. J_{pl}/J_{el} dependence from the remote stress.

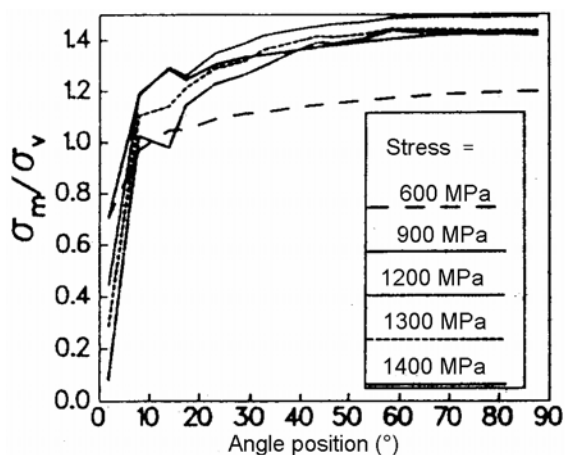


Figure 7. The change of LC along the crack front for an SCT specimen.

Other two examples calculated using ADINA programme, /6/, are also related to cylindrical pressured vessels ($D = 1500$ mm, $t = 40$ mm), with different axial cracks ($2a = 180.4$ mm and $c = 21.6$ mm for vessel PV1, $2a = 192.1$ mm and $c = 28$ mm for vessel PV2). The material and geometri-

cal nonlinearities were taken into account, but crack growth was not. In order to take crack growth into account, the obtained values of J integral were corrected according to the needed work of external forces, Fig. 9a for PV1 and 9b for PV2. Apparently, J integral distribution changes with pressure growth in such a way that local maximums occurs at approximately two thirds from the crack centre ($\phi = 60^\circ$), and in case of PV2 their values are greater than those of the maximums at the centre of the crack, Fig. 9b. The same goes for crack tip opening (δ), Fig. 10. The appearance of local maximums is even more pronounced in case of the distribution of local constraint (given by LC, Fig. 11 or as $J/\delta R_{el}$, Fig. 12). A more detailed view of these results as well as the experimental data are given in /1/.

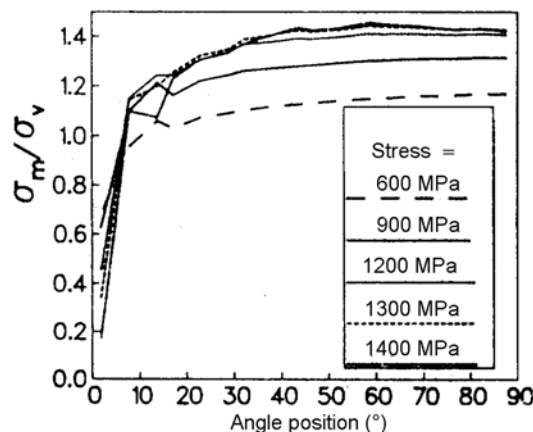


Figure 8. The change of LC along the crack front for a cylinder.

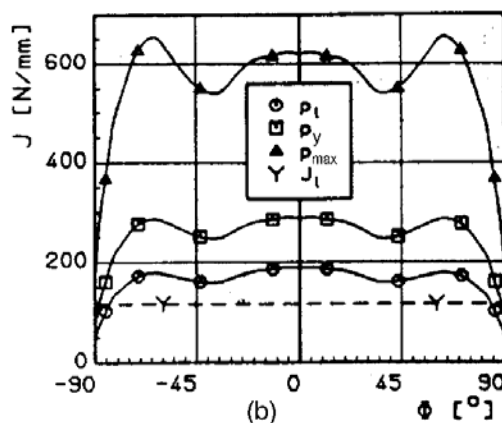
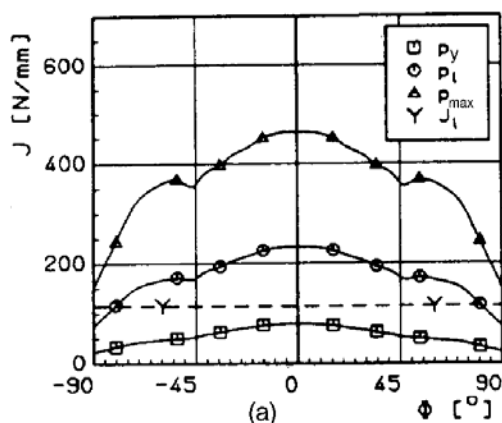


Figure 9. The change of J integral along the crack front.

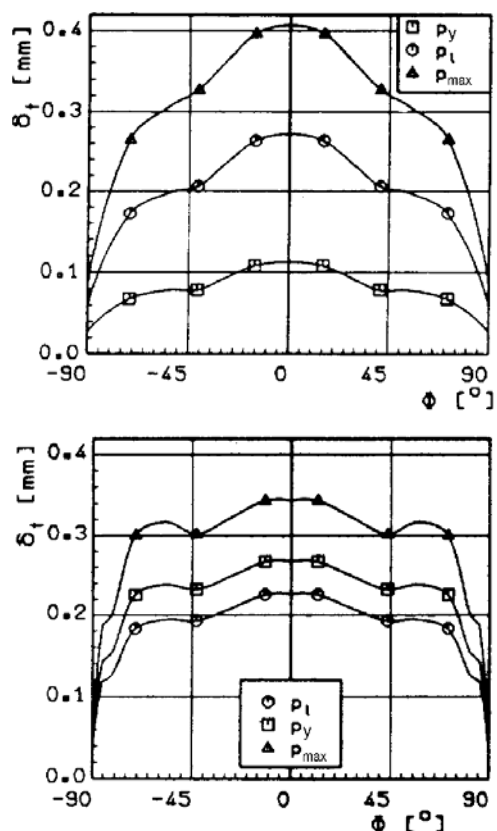


Figure 10. The change of δ_t along the crack front.

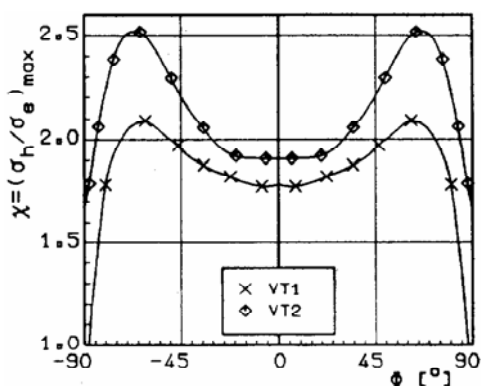


Figure 11. The change of LC along the crack front.

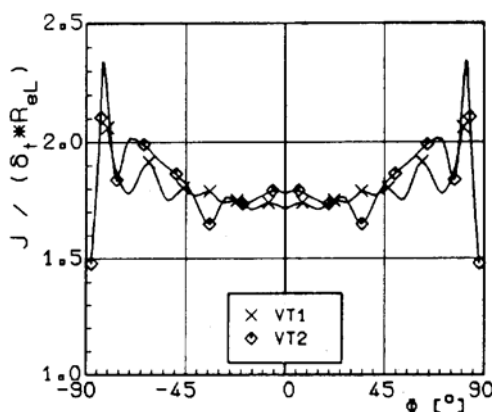


Figure 12. The change of J integral along the crack front.

Similar J integral and LC factor behaviour is shown in [9], which analyzes a surface crack ($2a = 28$ mm, $c = 12.6$ mm)

in a flat plate ($t = 20$ mm, $W = 60$ mm, $L = 300$ mm) also without crack growth simulation. The results are shown in Fig. 13 (J integral) and in Fig. 14 (LC), and Fig. 15 shows the finite element mesh. Again, in this case local maximums appear at approximately the same positions along the crack front ($\phi = 60^\circ$), although the stress state is not biaxial.

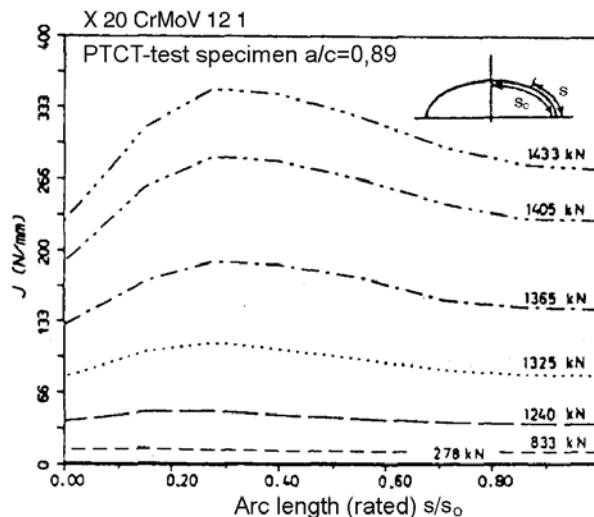


Figure 13. The change of J integral along the crack front.

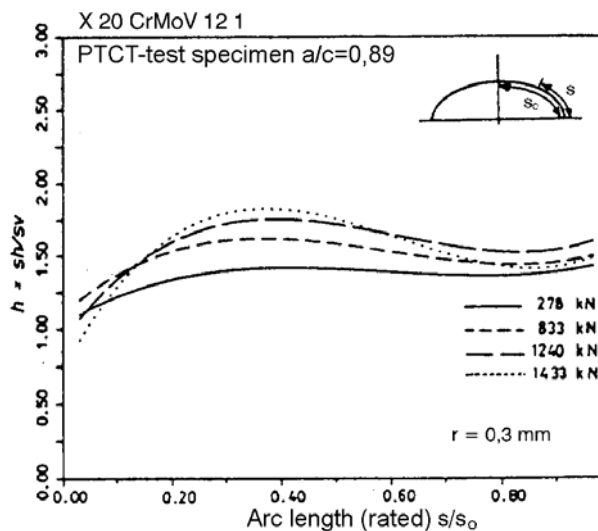


Figure 14. The change of LC along the crack front.

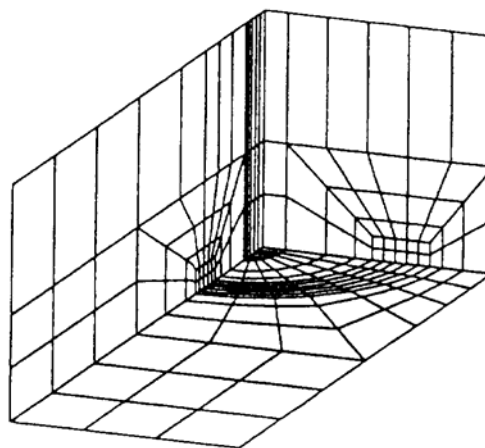


Figure 15. The finite element mesh.

QUASI-TWO DIMENSIONAL ANALYSIS

Given in this chapter are the basics of two methods of quasi-2D analysis of the problem of surface cracks in pressure vessels in the shape of thin shells. These methods are: the integral transformation method (model Ratwani-Erdogan-Irwin, REI) and the finite element method, combined with the line-spring model. Detailed description of REI model was given in previous Summer Schools, e.g. /10/, therefore this paper contains only a short review. It is about an elastic-plastic analysis of thin cylindrical shells with an axial crack which can be simplified in order to form and solve integral equations. The following basic assumptions are used to simplify the problem: the shape of the crack is rectangular (constant crack depth), there is no transversal shear (the Kirchoff theory is valid for thin shells) and the material is of ideal plasticity. Based on these assumptions, Dugdale's model of plastic strips in front of the crack tip can be applied. The solution of a problem defined in this way is given as a crack tip opening δ_i function of coordinates X (in the direction of the crack) and Z (in the direction of depth):

$$\delta_i(X, Z) = \delta(X, 0) + \theta(X)Z \quad (3)$$

Therefore, if we need the crack depth growth force (CGF) we should take the value of $\delta(X, c)$ and in case of crack length growth we choose the value $\delta(a, 0)$. It should be mentioned that CGF is determined using the J integral, based on the relation $J = mR_e\delta$, where $m = 2$ for all ideal plastic materials. Such an analysis was conducted in /11/, where CGFs were calculated for both cases (depth and length growth) and compared to the corresponding J-R curve. The problem of an axial crack ($2a = 64.25$ mm, $c = 11.2$ mm) in a cylindrical vessel ($D = 1200$ mm, $t = 16$ mm) previously examined experimentally and quasi-statically up to pressure value 134 bar, was analysed. At this value, the crack length increased ($2a = 80$ mm), while there was no increase in depth, Fig. 16. In order to explain such crack behaviour the REI model was applied and the results are shown in Fig. 17 (CGF for depth) and in Fig. 18 (for length). We can see from Fig. 17 and 18 that critical pressures for depth and length CGF equal 141 and 130 bar, respectively, which is in accordance with experimental behaviour.

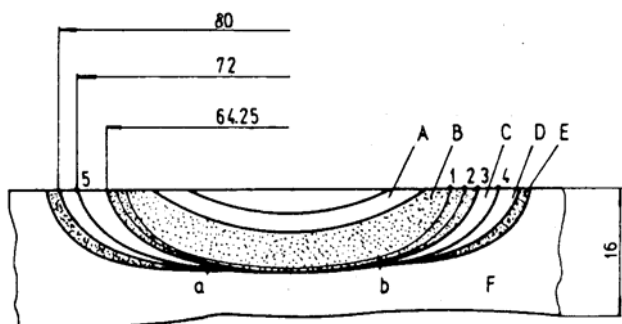


Figure 16. Cracked surface scheme.

The REI model basic advantage is its simple application, due to the fact that all the data needed for calculation are given in nondimensional form for characteristic nondimensional parameter values λ , where λ is defined as:

$$\lambda = \sqrt[4]{12(1-\nu^2)} \frac{2a}{\sqrt{Rt}}$$

Having in mind the assumptions made, we cannot expect significant accuracy from this model. However, in the analysed example, the efficiency of this model is apparent.

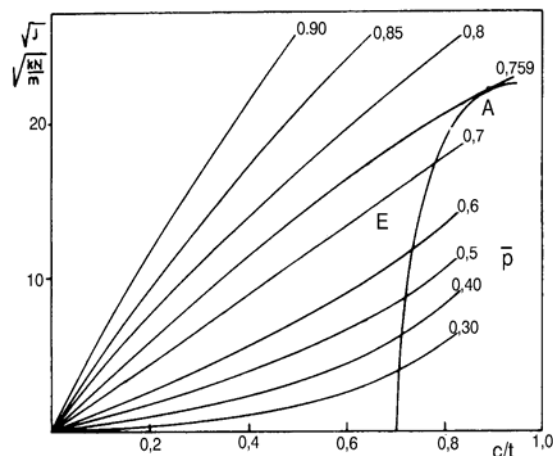


Figure 17. Development forces for constant crack length.

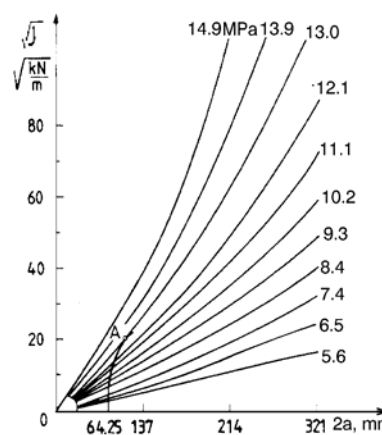


Figure 18. Development forces for constant crack depth.

LINE-SPRING MODEL – LSM

A very efficient surface crack analysis method was introduced in /12/. The basic idea is given in Fig. 19, which shows a way to solve a 3D problem using a combination of 2D problems (plane state of stress and strain). In other words, if the crack is temporary (along its entire thickness), the problem would be 2D (plane stress state – PSS), and if the surface crack length was equal to plate width, the problem would have been reduced to a plane strain state – PSS. Considering that a surface crack is something in-between these two extremes, the required solution can be obtained by combining 2D solutions. For this purpose, due to the existence of a residual ligament $t - c(x)$, Fig. 19a, the solution of the PSS problem must take into account local membrane $N(x)$ and bending $M(x)$ forces that appear on the crack surface. In order to determine the values of these forces, LSM relates them to corresponding movements, $\delta(x)$ and $\theta(x)$:

$$\begin{Bmatrix} \delta(x) \\ \theta(x) \end{Bmatrix} = \begin{bmatrix} C_{11}(x) & C_{12}(x) \\ C_{21}(x) & C_{22}(x) \end{bmatrix} \begin{Bmatrix} N(x) \\ M(x) \end{Bmatrix} \quad (4)$$

where $C_{ij}(x)$ are coefficients of the local stiffness matrix. As symbol (x) suggests, all quantities in [3] depend on the coordinate x , i.e. they change along the crack. Coefficients $C_{ij}(x)$ can be determined by solving the PSS problem (plate with an edge crack – Fig. 19c). This is a general description and in order to separate the problems of surface cracks in plates and shells as well as the elastic and elastic-plastic material behaviour, we will show each procedure apart:

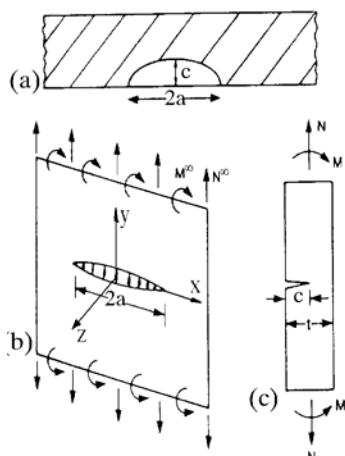


Figure 19. Line-spring model.

The following procedure is used for linear elastic flat plates:

- Coefficients $C_{ij}(x)$ are calculated from the solutions of the PSS problem for an edge crack in a flat plate, Fig. 19, $x < c$, using the Handbook /13/.
- The PSS problem is solved including the additional compliances $C_{ij}(x)$ on crack faces, e.g. by using the finite element method, in order to determine $\delta(x)$ $\theta(x)$.
- The values of forces $N(x)$ and $M(x)$ are determined from:

$$\begin{Bmatrix} N(x) \\ M(x) \end{Bmatrix} = [C]^{-1} \begin{Bmatrix} \delta(x) \\ \theta(x) \end{Bmatrix} \quad (5)$$

- The stress intensity factor is calculated:

$$K(x) = \sqrt{\pi C(x)} \left[F_1(c) \frac{N(x)}{t} + F_2(c) \frac{M(x)}{t^2/6} \right] \quad (6)$$

where $F_1(c)$ and $F_2(c)$ represent nondimensional functions which can be determined using Handbook /13/ for PSS tensile and bent plates with an edge crack.

It should be mentioned that this procedure, like any other concerning the LSM, cannot give satisfying results near the edge of the crack and surface, i.e. $\phi \rightarrow 0$.

The procedure used for linear elastic thin shells is similar to the above:

- Coefficients $C_{ij}(x)$ are calculated from PSS solutions for an edge crack in a ring, $x < c$, using /13/.
- The thin shell problem is solved including the additional compliances $C_{ij}(x)$ on crack faces, e.g. by using FEM.
- The values of forces $N(x)$ and $M(x)$ are determined along the crack faces based on [5].
- $K(x)$ is calculated from [6], while $F_1(c)$ and $F_2(c)$ are calculated using a ring instead of a plate.

As we can see, the basic difference between solving problems of surface cracks in a flat plate and in a thin shell by using the LSM is in step 2 of the given procedures, where in one case it is required to solve a PSS problem, and in the other case, it is required to solve a thin shell problem.

Elastic-plastic problems can be solved using the following procedure (related to flat plates and thin shells):

- Incremental elastic-plastic coefficients $C_{ij}(x)$ for an edge crack are calculated in a flat plate or a ring, using FEM or the Handbook, /14/.
- The elastic-plastic PSS problem for a plate or a thin shell is solved (using FEM) in order to obtain incremental values of $\delta(x)$ and $\theta(x)$.
- Incremental values of $N(x)$ and $M(x)$ are determined using [5].
- $J(x)$ is calculated from an incremental elastic-plastic solution of a PSS problem for an edge crack in a plate or a ring, using FEM or /14/.

The procedure described above is obviously complicated yet much simpler than the complete 3D solution. These two solutions are in good accordance with each other (except for $\phi \rightarrow 0$), as Figs. 20 and 21 suggest.

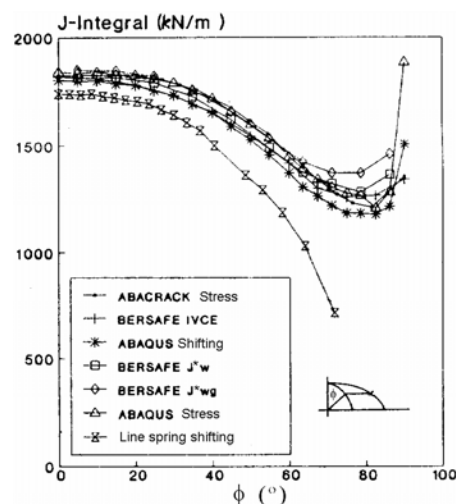


Figure 20. The change of elastic-plastic J integral around the crack tip.

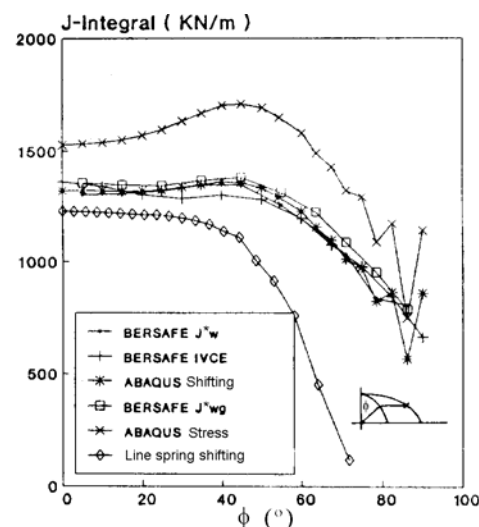


Figure 21. The change of elastic-plastic J integral around the crack tip.

Very significant for this procedure is that it also analyses heterogeneous material, such as welded joints which have at least three different types of material behaviour: the basic metal – BM, the weld metal – WM and the heat affected zone – HAZ. We should notice that the possibility of analysing such materials is connected to the application of FEM and that different behaviour becomes distinct in the plastic domain. Therefore, the problem of J integral independence from the path should be taken into account. An example of such analysis is given in [16], which shows that a modified J integral can be used as a fracture mechanics parameter for welded joints.

THE SIMPLIFIED KING LINE-SPRING MODEL

Although King's model is described in other papers, e.g. [20], all fundamental expressions are also given here, mainly for two reasons. First, the efficiency of applying this model in engineering which is, according to the author, most expressed in large spheres, and the second reason are the mistakes that appear in some expressions given in the mentioned references.

Fundamental assumptions of King's model are the following:

- The surface crack is located in an infinite flat tensile plate, loaded by a remote stress σ .
- The real crack front is replaced by a rectangular one, with a constant crack depth, $c = \text{const}$.
- The spring is elastic and ideally plastic.
- Dugdale's model is applied so that we can take into account plasticity around the crack tip of a temporary crack.

Therefore, σ being the remote stress, $\sigma_c = N/h$ – the membrane load and $m = M/(h^2/6)$ – bending load, we write:

$$\delta = \frac{4a}{E} (\sigma - \sigma_c) \quad (7)$$

$$\theta = \frac{-8(1+\nu)a}{(3+\nu)Eh} m \quad (8)$$

On the other hand, it is obvious that:

$$\delta = \frac{2(1-\nu^2)h}{E} (C_{11}\sigma_c + C_{12}m) \quad (9)$$

$$\theta = \frac{12(1-\nu^2)}{E} (C_{12}\sigma_c + C_{22}m) \quad (10)$$

By eliminating δ and θ from equations [7], [8], [9] and [10], we obtain:

$$\sigma_c = \frac{2}{1-\nu^2} \frac{a}{hD} \left[C_{22} + \frac{2}{3(1-\nu)(3+\nu)} \frac{a}{h} \right] \sigma = \alpha \sigma \quad (11)$$

$$m = -\frac{2}{1-\nu^2} \frac{a}{hD} C_{12} \sigma = -\beta \sigma \quad (12)$$

where:

$$D = \left(C_{11} + \frac{2}{1-\nu^2} \frac{a}{h} \right) \left[C_{22} + \frac{2}{3(1+\nu)(3+\nu)} \frac{a}{h} \right] - C_{12}^2 \quad (13)$$

The spring remains elastic until it reaches the yield limit. A simple expression is used as a yield criterion, and it is shown that this expression complies with experimental data [21,22]:

$$\sigma_c = \frac{h-c}{h} \sigma_F \quad (14)$$

Equation [14] is understood as the yielding occurs when the average stress in a ligament reaches the value of the flow (hardening) stress, σ_F , defined as:

$$\sigma_F = \frac{\sigma_Y + \sigma_m}{2} \quad (15)$$

Equation [14] gives us the expression for the stress at the instant yielding in the ligament occurs:

$$\sigma_{LY} = \frac{1}{\alpha} \left(1 - \frac{c}{h} \right) \sigma_F \quad (16)$$

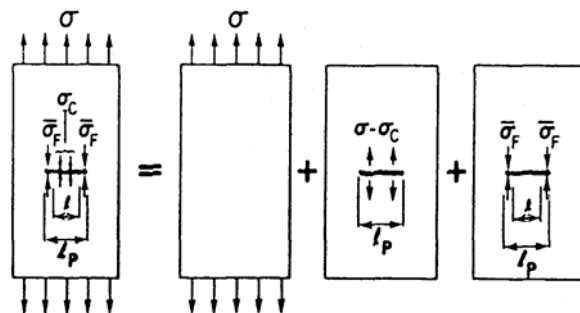


Figure 22. Solving the yield strips for a plate of finite width.

After yielding, the plasticity in temporary crack tips is taken into account using "effective" crack length, $a_p = a + r_v$, where r_v represents the dimension of the plastic zone*. Hence, by using Dugdale's model of loading strips, Fig. 22, we obtain:

$$\sin \frac{\pi a_p}{w} = \frac{\sin \frac{\pi a}{w}}{\cos \frac{\pi}{2} \frac{\sigma - \sigma_c}{\sigma_F - \sigma_c}} = \frac{\sin \frac{\pi a}{w}}{\cos \frac{\pi}{2} \left[\frac{h}{c} \frac{\sigma}{\sigma_F} - \left(\frac{h}{c} - 1 \right) \right]} \quad (17)$$

where w represents plate width. The plate can hold the load until the yield strips reach its edges, which is defined using the net section yield stress σ_{NSY} , obtained from [17] by placing $a_p = w/2$:

$$\sigma_{NSY} = \sigma_F \left(1 - \frac{2a}{w} \frac{c}{h} \right) \quad (18)$$

It should be mentioned here that King's model applies to plates of finite width. However, in case that $w \rightarrow \infty$, $\sin(\pi a_p/w) \approx \pi a_p/w$ and $\sin(\pi a/w) \approx \pi a/w$, an approximate solution of the problem is obtained for an infinite plate:

$$a_p = \frac{a}{\cos \frac{\pi}{2} \left[\frac{h}{c} \frac{\sigma}{\sigma_F} - \left(\frac{h}{c} - 1 \right) \right]} \quad \text{and} \quad \sigma_{NSY} \approx \sigma_F \quad (19)$$

which is applicable to thin shells with small curves, e.g. in large spheres. As the σ_c and m are defined for an entire range of remote stress σ , COD and J can be determined. From Fig. 23 we have:

$$\text{CTOD} = \delta + \theta(h - 2C) \quad (20)$$

$$\text{CMOD} = \delta + \theta h \quad (21)$$

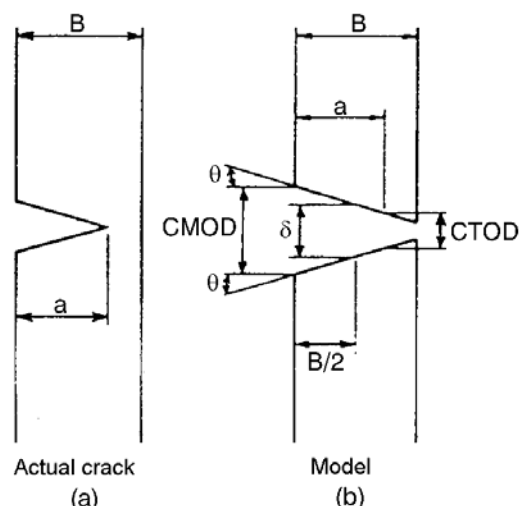


Figure 23. Calculation of CMOD and CTOD.

By placing the expression for δ and θ we get ($\sigma \leq \sigma_{LY}$)

$$CTOD = \frac{4a\sigma}{E} \left[1 + \left(\frac{2(1+\nu)}{3+\nu} \frac{h-2C}{h} \beta - \alpha \right) \right] \quad (22)$$

$$CMOD = \frac{4a\sigma}{E} \left[1 + \left(\frac{2(1+\nu)}{3+\nu} \beta - \alpha \right) \right] \quad (23)$$

i.e. (for $\sigma_{LY} \leq \sigma \leq \sigma_{NSY}$):

$$CTOD = \frac{4(a+r_y)}{E} (\sigma - \sigma_{LY}) + CTOD_{LY} \left(\frac{a+r_y}{a} \right) \quad (24)$$

$$CMOD = \frac{4(a+r_y)}{E} (\sigma - \sigma_{LY}) + CMOD_{LY} \left(\frac{a+r_y}{a} \right) \quad (25)$$

In order to calculate J , for $\sigma < \sigma_{LY}$ we can use LEMLEFM relations:

$$J_c = \frac{1-\nu^2}{E} K_I^2 = \frac{1-\nu^2}{E} h (\sigma_c F_1 + m F_2)^2 \quad (26)$$

where F_1 and F_2 are given by:

$$F_1(x) = \sqrt{\pi x} (1.12 + 6.52x^2 - 12.39x^4 + 89.05x^6 - 188.61x^8 + 207.39x^{10} - 32.05x^{12})$$

$$F_2(x) = \sqrt{\pi x} (1.12 - 1.89x + 18.01x^4 - 87.39x^3 + 241.9x^4 - 319.94x^5 - 168.01x^6)$$

For $\sigma_{LY} < \sigma < \sigma_{NSY}$, J_p is calculated using the movement of load line contact on the edge of the crack:

$$J_p = - \int_{\delta_{LY}}^{\delta} \frac{\partial N}{\partial c} d\delta - \int_{\theta_{LY}}^{\theta} \frac{\partial M}{\partial c} d\theta \quad (27)$$

where, for $\partial N / \partial c = -\sigma_F$, $\partial M / \partial c = 0 \Rightarrow$

$$J_p = \sigma_F (\delta - \delta_{LY}) = \frac{4\sigma_F}{E} \left[(a+r_y) \sigma - a\sigma_{LY} - \frac{h-c}{h} r_y \sigma_F \right] \quad (28)$$

The example which illustrates the application of King's LSM in case of a spherical tank for butane-propane is given in /23/, while the final result is shown here as a CGF diagram, Fig. 24.

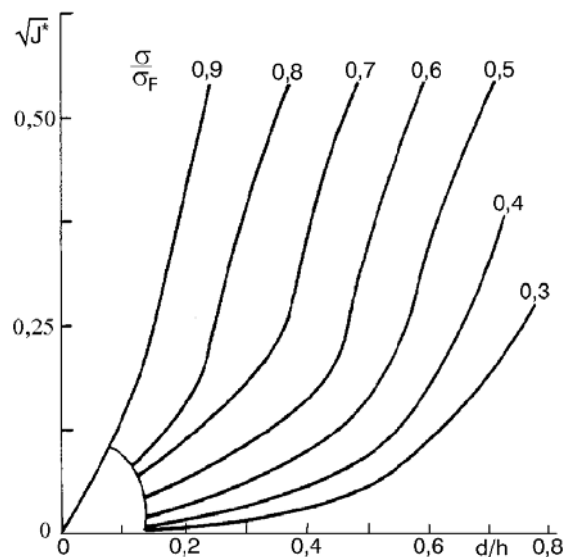


Figure 24. Crack development forces for a spherical vessel according to LSM

TWO-DIMENSIONAL ANALYSIS

As mentioned previously, in case of long and shallow cracks, 2D analysis (PSS gives satisfying approximate solutions. Such analysis can simply be conducted by using a modified programme /24/ with the application of recommendations of the European Structural Integrity Society (ESIS) given in monograph /25/. Solving the elastic-plastic 2D problem of fracture mechanics was already described, /26/, therefore, here we will only mention that the entire calculation can be done using a personal computer.

AN EXAMPLE

In order to illustrate and compare the analysis of some described procedures for solving the problem of surface cracks in a pressure vessel, we have chosen a cylinder (diameter $D = 120$ mm, thickness $t = 5$ mm), made of steel with following properties: ultimate strength $R_m = 1350$ MPa, yield strength $R_{p0.2} = 1175$ MPa, elasticity modulus $E = 210$ GPa, Poisson's ratio $\nu = 0.3$, shear modulus $E = 3000$ MPa. The problem was solved using a REI model, a simplified King model, LSM combined with the thin shells theory described in /27/, as well as the PSS 2D problem. The finite element mesh for the last method mentioned was shown in Fig. 25. The following data are required:

- 8-node iso-parametric elements with Gauss integration of 2×2 were used,
- singularity around the crack tip (type $1/r$) was modelled by triangular elements with three independent nodes near the crack tip,
- a finite element mesh was given in accordance with ESIS,
- the material was given as bilinear, with previously given properties.

Results for all of the methods were given in Fig. 26 in a form of diagrams of CGF dependence to crack depth. As we can see from Fig. 26, mutual compliance of the methods described is satisfying within quasi-two dimensional analysis (REI, King's model, LSM and thin shell theory), with significant deviations in results of two dimensional analysis

(FEM). In case of 2D analysis, the crack growth force is much greater than the others, which results from modelling of the surface crack with a crack along the entire plate width, i.e. vessel length. Similar results, along with the same discussion, are given in /28/. It is clear that the 2D analysis may serve only as a conservative approach in determining crack growth forces. Also, a greater surface crack length-to-plate width ratio (vessel depth) results in greater accuracy of this analysis. Apparently, a more accurate assessment using finite element method can be made only by applying 3D analysis, which of course increases the calculating expenses.

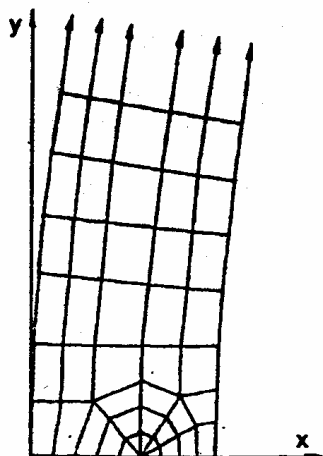


Figure 25. A finite element mesh.

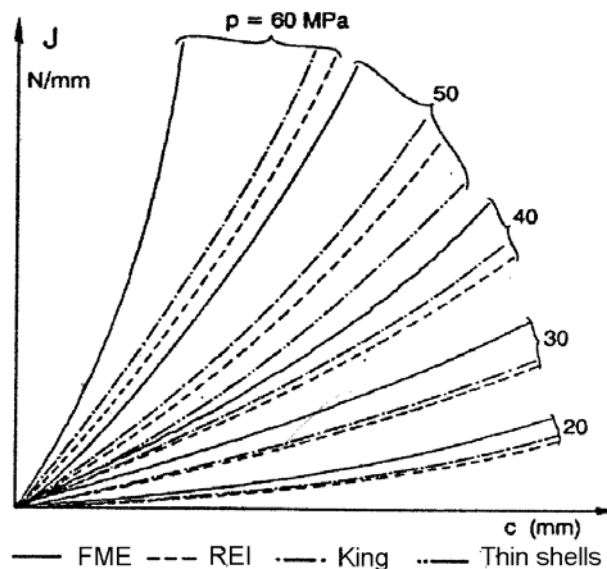


Figure 26. Crack growth forces for the cylindrical vessel.

REFERENCES

- Brocks, W., *Ispitivanje i analiza realnih posuda pod pritiskom*, Monografija 6. MLŠML, Vrdnik, 1991, TMF-GOŠA, str. 37
- Radon, J., *Nastanak i rast zamornih prslina u posudama pod pritiskom*, ibid 1, str. 52.
- Mazur, A., *Naponska korozija specijalnih čelika srednje i povišene čvrstoće*, ibid 1, str. 52.
- Raju, I.S., Newman, J.C., *Stress intensity factors for a wide range of semi-elliptical surface cracks in finite thickness plates*, Eng. Fracture Mech. 11, 1979, 817-829.
- Newman, J.C., Raju, I.C., *Stress intensity factors for internal surface cracks in cylindrical pressure vessel*, Trans. ASME, J. Pressure Vessel Technology 102, 1980, 342-346.
- Brocks, W. et al., *Ductile crack growth of semi-elliptical surface flaws in pressure vessels*, Int. J. Pres. Vess. & Piping 43, 1990, 301-316.
- Brocks, W. et al., *On the transferability of fracture mechanics parameters from specimens to structures using FEM*, Nuclear Engineering and Design 112, 1989, 1-14.
- Agatonović, P., Windisch, M., *Non-linear fracture mechanics analysis of specimens and components with surface cracks*, Proc. 5th Int. Conf. NMFm, Pineridge Press, Freiburg, 1990, 597-610.
- Siegele, D., Computers & Structures 32, No 3/4, 1989, 639.
- Ratwani, M.M., Monografija 2, MLŠML, 1982.
- Sedmak A., Sedmak S., Jokanović, Z., *Numerical analysis of crack behavior in the full-scale pressure vessel test*, Proc. 5th Int. Conf. NMFm, Pineridge Press, Freiburg, 1990, 611-618.
- Rice, J.R., Levy, N., *The part-through surface crack in an elastic plate*, J. Appl. Mech. 39, 1972, 185-194.
- Tada, H., Paris, P., Irwin, G., *The stress analysis of cracks - Handbook*, Del Research Corporation, Hellertown, Penn. 1973.
- Kumar, V., German M.D., Shih, C.F., *An engineering approach for elastic-plastic fracture mechanics analysis*, Report No. EPRI NP-1931, RP 1237-1, General Electric, Schenectedy, 1981.
- Marsden, B.J. et al., *Elasto-plastic analysis of semi-elliptical defect in a wide plate*, Proc. 5th Int. Conf. NMFm, Pineridge Press, 1991, 569-583.
- Sedmak, A., Sedmak, S., Vukomanović, N., Proc. ECF 8, Torino, EMAS, 1990, 15961-1599.
- Parks, D.M., *Inelastic analysis of surface flaws using the line-spring model*, Proc. ICF 5, Pergamon Press, Oxford, 1981, 2589-2598.
- Erdogan, F., Aksel, B., *Line spring model and its application to part-through crack problems in plates and shells*, ASTM STP 969, 1988, 125-152.
- Kumar, V., German, M.D., *Studies on the line spring model for nonlinear crack problems*, Computational Fracture Mechanics - Nonlinear and 3-D Problems, ASME, San Antonio, 1984, 1-24.
- King, R.B., *Elastic-plastic analysis of surface flaws using a simplified line-spring model*, Eng. Fracture Mech. 18, 1983, 217-231.
- King, R.B., Cheng, Y.W., Read, D.T., *J-integral analysis of surface flaws in pipeline steel plates*, 2nd Int. Symp. Elastic-Plastic Fracture Mechanics, Philadelphia, 1981.
- Cheng, Y.W., McHenry, H.I., *Crack opening displacement of surface cracks in pipeline steel plates*, ASTM XIV Symp, Fracture Mechanics, L.A., 1981.

23. Sedmak, S., Petrovski, B., Sedmak, A., Lukačević, Z., *The study of crack significance in spherical storage tanks by J-resistance curve*, Int. Conf. on Weld Failures, Welding Institute, London, 1988, P18-1-10.
24. Owen, D.R.J., Fawkes, J., *Fracture mechanics engineering*, Pineridge Press, Swansea, 1984.
25. Savović, N., Sedmak, A., *Preporuke za primenu metode konačnih elemenata na probleme mehanike loma*, ibid 1, str. 229.
26. Sedmak, A., Ogarević, V., Kovačević, J., *Određivanje parametara elastoplastične mehanike loma*, Monografija 4, MLŠML, Arandelovac, 1984, str. 301.
27. Sedmak, A., *Zakon održanja tipa J integrala za tanke ljuske*, Doktorska teza, PMF, Univerzitet u Beogradu, 1988.
28. Killian, D.E., Yoon, K.K., *Elastic-plastic Analysis of Reactor Vessel Longitudinal Flaws*, ASTM STP 1131, Vol. 1, 1992, 248-267.